Proceedings of The Fourteenth (2004) International Offshore and Polar Engineering Conference
Toulon, France, May 23–28, 2004

ISBN 1-880653-62-1 (Set); ISSN 1098-6189 (Set)

Strengthening of Square Reinforced Concrete Plates with Fiber Reinforced Plastics

Fu-Ming Lin and Hsuan-Teh Hu
Department of Civil Engineering, National Cheng Kung University
Tainan, TAIWAN, China

ABSTRACT

This paper presents a reasonable numerical model for reinforced concrete structures strengthened by FRP. Proper constitutive models are introduced to simulate the nonlinear behaviors of reinforced concrete and FRP. The finite element program ABAQUS is used to perform the nonlinear failure analysis of the discussed problems. The validity of proposed material models is verified with experimental data and some strengthening schemes are discussed in detail for engineering applications. It has been shown that the use of fiber-reinforced plastics can significantly increase the stiffness as well as the ultimate strengths of reinforced concrete slabs. In addition, the nonlinearity of FRP in in-plane shear stress-strain relation dose not influence the behavior of such composite slabs, because of the small failure shear strain of the composite plates.

KEYWORDS: Two-way slab; FRP composites; Retrofit; Strengthened; Nonlinear finite element analysis

INTRODUCTION

The traditional material used in the strengthening of concrete structures is steel. Because of its drawbacks of low corrosion resistance and of handling problems involving excessive size and weight, there is a need for the engineering community to look for alternatives. Due to the advantages of high strength-to-weight ratio, excellent resistance to electrochemical corrosion and good fatigue strength, fiber reinforced plastics (FRP) have become attractive materials in the repairing and strengthening of the structures (Saadatmanesh and Ehsani, 1991).

In recent years, numerous researches were carried out experimentally and analytically to investigate the performance of concrete structures with bonded external composite materials. But almost of them were focused mainly on the beam and column members.

To study the behavior of reinforced concrete structures strengthened by FRP, the fundamental step is to understand the nonlinear behavior of the constitutive materials, reinforced concrete and FRP, separately. The nonlinear behavior of reinforced concrete such as concrete cracking, tension stiffening, shear retention, concrete plasticity and yielding of reinforcing steel have been extensively studied by various researchers and numerous proper constitutive laws have been proposed (Hu and Schnobrich, 1989; 1990; Vecchio and Collins, 1986). However, in the literature, most studies of reinforced concrete structures strengthened by FRP have assumed that the behavior of FRP is linear. It is well known that unidirectional fibrous composites exhibit severe nonlinearity in their in-plane shear stress-strain relations (Hahn and Tsai, 1973). In addition, deviation from linearity is also observed with in-plane transverse loading but the degree of nonlinearity is not comparable to that observed with the in-plane shear (Hahn and Tsai, 1973; Jones and Morgan, 1977). Also, due to the relative volume fractions of fiber and matrix, the composite stress-strain curves will display nonlinear characteristics to some extent both in longitudinal and transverse direction. Therefore, appropriate modeling of the nonlinear behavior of FRP becomes crucial.

In this investigation, proper constitutive models are introduced to simulate the nonlinear behavior of reinforced concrete and FRP. Then the finite element program ABAQUS is used to perform a failure analysis of rectangular reinforced concrete slabs strengthened by FRP. One aim of this research is to establish a reasonable nonlinear FE numerical model by considering more realistic material properties. To verify the proposed constitutive models, we compare the numerical results with experimental data. And the good agreements can be shown between them.

MATERIAL PROPERTIES AND CONSTITUTIVE MODELS

The materials used in the analysis involve steel reinforcing bars, concrete and fiber-reinforced plastics. Reliable constitutive models applicable to steel reinforcing bars and concrete are available in the ABAQUS material library. Thus, their input material properties and associated constitutive models are only briefly discussed. The ABAQUS program does not have a nonlinear material library for FRP. Hence, its nonlinear constitutive model is discussed here in detail. The resulting nonlinear constitutive equations for the FRP are coded in FORTRAN language as a subroutine and linked to the ABAQUS program.

Steel Reinforcing Bar

The tress-strain curve of reinforcing bar is assumed to be elastic perfectly plastic. The elastic modulus is assumed to be 199.9 GPa (29000 ksi) and the yielding stress is assumed to be 413.7 GPa (60 ksi). The curve is as shown in Fig.1.

In ABAQUS, the steel reinforcement is treated as an equivalent uniaxial material smeared through out the element section and the bond-slip effect between concrete and steel is not considered. In order to properly model the constitutive behavior of the reinforcement, the cross sectional area, spacing, position and orientation of each layer of steel bar within each element needs to be specified.

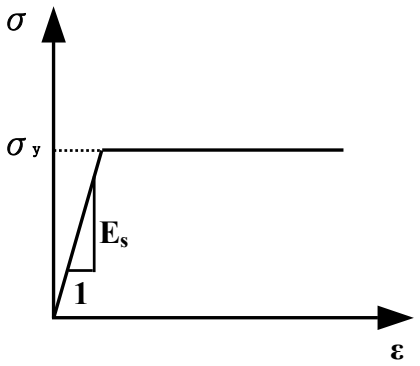

Fig. 1. Elastic perfectly plastic model for reinforcing bar.

Concrete

The uniaxial compressive strength of concrete is selected as

$$f_c^{'} = 34.47 \quad \text{MPa} \quad (5 \text{ ksi}) \tag{1}$$

Under uniaxial compression, the concrete strain ε_o corresponding to the peak stress $f_c^{'}$ is usually around the range of 0.002 to 0.003. A representative value of ε_o suggested by ACI Committee 318 (ACI318-99, 1999) and used in the analysis is

$$\varepsilon_o = 0.003 \tag{2}$$

The Poisson's ratio ν_c of concrete under uniaxial compressive stress ranges from about 0.15 to 0.22, with a representative value of 0.19 or 0.20 (ASCE Task Committee on Concrete and Masonry Structure, 1982). In this study, the Poisson's ratio of concrete is assumed to be

$$\nu_c = 0.2 \tag{3}$$

The uniaxial tensile strength $f_t^{'}$ of concrete is difficult to measure. For this study the value is taken as (ASCE Task Committee on Concrete and Masonry Structure, 1982)

$$f_t^{'} = 0.33\sqrt{f_c^{'}} \quad \text{MPa} \tag{4}$$

The initial modulus of elasticity of concrete E_C is highly correlated to its compressive strength and can be calculated with reasonable accuracy from the empirical equation (ACI318-99, 1999)

$$E_C = 4700\sqrt{f_c^{'}} \quad \text{MPa} \tag{5}$$

Under multiaxial combinations of loading, the failure strengths of concrete are different from those observed under uniaxial condition. However, the maximum strength envelope under multiple stress conditions seems to be largely independent of load path (Kupfer, Hilsdorf, and Rusch, 1969). In ABAQUS, a Mohr-Coulomb type compression surface together with a crack detection surface is used to model the failure surface of concrete (Fig. 2). When the principal stress components of concrete are predominantly compressive, the response of the concrete is modeled by an elastic-plastic theory with an associated flow and an isotropic hardening rule. In tension, once cracking is defined to occur (by the crack detection surface), the orientation of the crack is stored. Damaged elasticity is then used to model the existing crack (Hibbitt, Karlsson, and Sorensen, 2002).

When plastic deformation occurs, there should be a certain parameter to guide the expansion of the yield surface. A commonly used approach is to relate the multidimensional stress and strain conditions to a pair of quantities, namely, the effective stress σ_c and effective strain ε_c, such that results obtained following different loading paths can all be correlated by means of the equivalent uniaxial stress-strain curve. The stress-strain relationship proposed by Saenz (1964) has been widely adopted as the uniaxial stress-strain curve for concrete and it has the following form

$$\sigma_C = \frac{E_C \varepsilon_C}{1 + (R + R_E - 2)(\frac{\varepsilon_C}{\varepsilon_o}) - (2R - 1)(\frac{\varepsilon_C}{\varepsilon_o})^2 + R(\frac{\varepsilon_C}{\varepsilon_o})^3} \tag{6}$$

where

$$R = \frac{R_E(R_\sigma - 1)}{(R_\varepsilon - 1)^2} - \frac{1}{R_\varepsilon}, \qquad R_E = \frac{E_C}{E_o}, \qquad E_o = \frac{f_c^{'}}{\varepsilon_o}$$

and $R_\sigma = 4$, $R_\varepsilon = 4$ may be used (Hu and Schnobrich, 1989). In the analysis, equation (6) is taken as the equivalent uniaxial stress-strain curve for concrete and approximated by several piecewise linear segments as shown in Fig. 3.

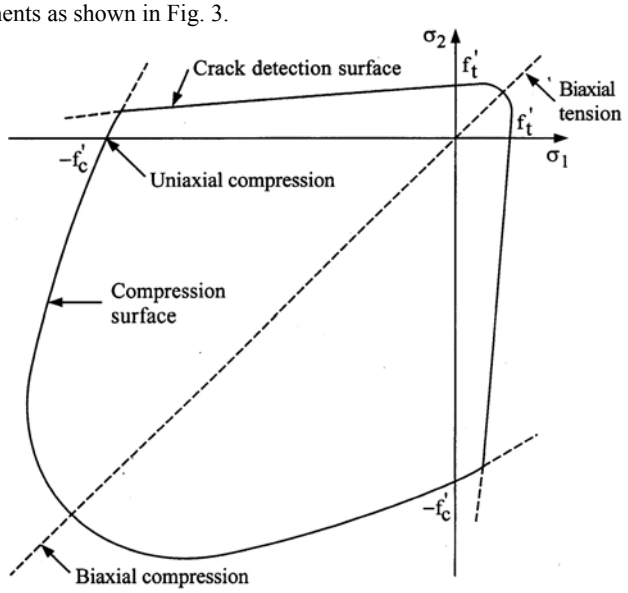

Fig 2. Concrete failure surface in plane stress

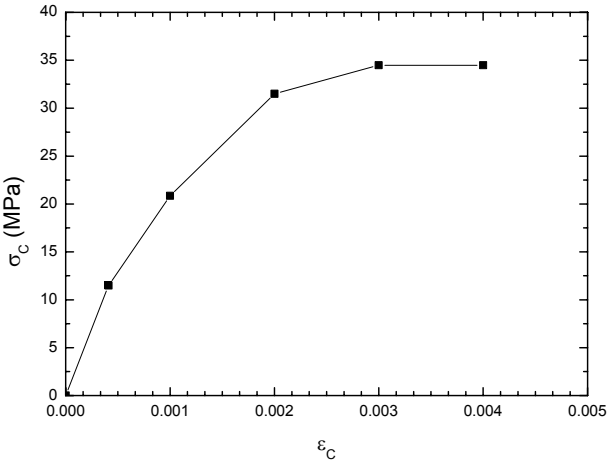

Fig. 3 Equivalent uniaxial stress-strain curve for concrete

When cracking of concrete takes place, a smeared model is used to represent the discontinuous macrocrack behavior. It is known that the cracked concrete of a reinforced concrete element can still carry some tensile stress in the direction normal to the crack, which is termed tension stiffening (ASCE Task Committee on Concrete and Masonry Structure, 1982). In this study, a simple descending line is used to model this tension stiffening phenomenon (Fig. 4). The value of the strain ε* at which the tension stiffening stress reduced to zero is 0.0006 determined by calibrating with the experimental data (Mosallam and Mosalam, 2003) in the analytical model.

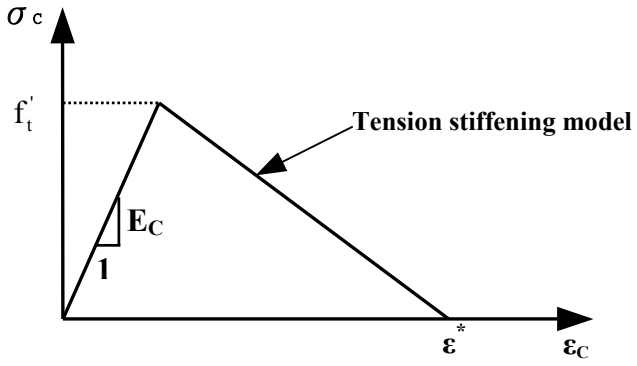

Fig. 4. Tension stiffening model

During the postcracking stage, the cracked reinforced concrete can still transfer shear forces through aggregate interlock or shear friction, which is termed shear retention. Assuming that the shear modulus of intact concrete is G_c, then the reduced shear modulus $\hat{G}$ of cracked concrete can be expressed as

$$\hat{G} = \mu G_C \tag{4}$$

$$\mu = 1 - \varepsilon / \varepsilon_{\max} \tag{5}$$

where ε is the strain normal to the crack direction and ε_{max} is the strain at which the parameter μ reduces to zero (Fig. 5). Numerous analytical results have demonstrated that the particular value chosen for μ (between 0 and 1) does not appear to be critical but values greater than zero are necessary to prevent numerical instabilities (Hu and Schnobrich, 1990). In ABAQUS, ε_{max} is usually assumed to be a very large value, i.e., μ = 1 (full shear retention). In this investigation, the default values for shear retention parameter μ = 1 are used.

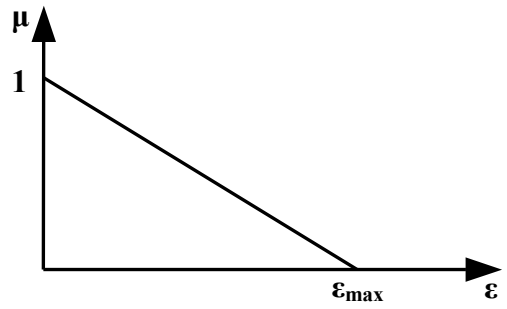

Fig. 5. Shear retention parameter

Fiber-Reinforced Plastics

For fiber-reinforced plastics (Fig. 6), each lamina can be considered as an orthotropic layer in a plane stress condition. It is well known that unidirectional fibrous composites exhibit severe nonlinearity in their in-plane shear stress-strain relation. In addition, deviation from linearity is also observed with in-plane transverse loading but the degree of nonlinearity is not comparable to that in the in-plane shear (Hahn and Tsai, 1973). Also, due to the relative volume fractions of fiber and matrix, the composite stress-strain curves will display nonlinear characteristics to some extent both in longitudinal and transverse direction. Usually, this nonlinearity associated with the transverse loading can be ignored (Jones and Morgan, 1977). To model the nonlinear in-plane shear behavior, the nonlinear strain-stress relation for a composite lamina suggested by Hahn and Tsai (1973) is adopted. Values are given as follows:

$$\begin{Bmatrix} \varepsilon_1 \\ \varepsilon_2 \\ \gamma_{12} \end{Bmatrix} = \begin{bmatrix} \frac{1}{E_{11}} & \frac{-\nu_{21}}{E_{22}} & 0 \\ \frac{-\nu_{12}}{E_{11}} & \frac{1}{E_{22}} & 0 \\ 0 & 0 & \frac{1}{G_{12}} \end{bmatrix} + S_{6666}\tau_{12}^2 \begin{Bmatrix} 0 \\ 0 \\ \tau_{12} \end{Bmatrix} \tag{6}$$

In this model only one constant S_{6666} is required to account for the in-plane shear nonlinearity. The value of S_{6666} can be determined by a curve fit to various off-axis tension test data (Hahn and Tsai, 1973). Let us define $\Delta\{\sigma'\} = \Delta\{\sigma_1,\sigma_2,\tau_{12}\}^T$ and $\Delta\{\varepsilon'\} = \Delta\{\varepsilon_1,\varepsilon_2,\gamma_{12}\}^T$. Inverting and differentiating Eq. (6), the incremental stress-strain relations are established

$$\Delta\{\sigma'\} = [Q_1']\Delta\{\varepsilon'\} \tag{7}$$

$$[Q_1'] = \begin{bmatrix} \frac{E_{11}}{1-\nu_{12}\nu_{21}} & \frac{\nu_{12}E_{22}}{1-\nu_{12}\nu_{21}} & 0 \\ \frac{\nu_{21}E_{11}}{1-\nu_{12}\nu_{21}} & \frac{E_{22}}{1-\nu_{12}\nu_{21}} & 0 \\ 0 & 0 & \frac{1}{1/G_{12} + 3S_{6666}\tau_{12}^2} \end{bmatrix} \tag{8}$$

Furthermore, it is assumed that the transverse shear stresses always behave linearly and do not affect the nonlinear behavior of any in-plane shear. If we define $\Delta\{\tau_t'\} = \Delta\{\tau_{13},\tau_{23}\}^T$ and $\Delta\{\gamma_t'\} = \Delta\{\gamma_{13},\gamma_{23}\}^T$, the constitutive equations for transverse shear stresses become

$$\Delta\{\tau_t'\} = [Q_2']\Delta\{\gamma_t'\} \tag{9}$$

$$[Q_2'] = \begin{bmatrix} \alpha_1 G_{13} & 0 \\ 0 & \alpha_2 G_{23} \end{bmatrix} \tag{10}$$

where α_1 and α_2 are the shear correction factors and are taken to be 0.83 in this study.

Among existing failure criteria, the Tsai-Wu criterion (Tsai and Wu,1971) has been extensively used in the literature and is adopted in this analysis. Under plane stress conditions, this failure criterion has the fol

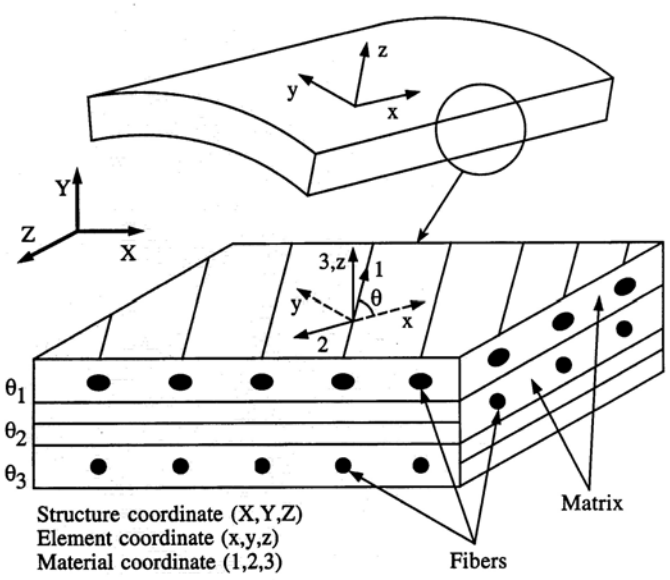

Fig 6. Material, element and structure coordinates of fiber reinforced plastics

$$F_1\sigma_1 + F_2\sigma_2 + F_{11}\sigma_1^2 + 2F_{12}\sigma_1\sigma_2 + F_{22}\sigma_2^2 + F_{66}\tau_{12}^2 = 1 \tag{11}$$

with

$$F_1 = \frac{1}{\overline{X}} + \frac{1}{\overline{X'}},\quad F_2 = \frac{1}{\overline{Y}} + \frac{1}{\overline{Y'}},\quad F_{11} = \frac{1}{\overline{X}\,\overline{X'}},\quad F_{22} = \frac{1}{\overline{Y}\,\overline{Y'}},\quad F_{66} = \frac{1}{\overline{S}^2}.$$

The $\overline{X}$, $\overline{Y}$ and $\overline{X}'$, $\overline{Y}'$ are the lamina longitudinal and transverse strengths in tension and compression, respectively, and $\overline{S}$ is the shear strength of the lamina. Though the stress interaction term F_{12} in Eq. (11) is difficult to be determined, it has been suggested that F_{12} can be set equal to zero for practical engineering applications (Narayanaswami and Adelman, 1977). Therefore, $F_{12} = 0$ is used in this investigation.

During the numerical calculation, incremental loading is applied to composite plates until failures in one or more of individual plies are indicated according to Eq. (17). Since the Tsai-Wu criterion does not distinguish failure modes, the following two rules are used to determine whether the ply failure is caused by resin fracture or fiber breakage (Rowlands, 1985):

(1) If a ply fails but the stress in the fiber direction remains less than the uniaxial strength of the lamina in the fiber direction, i.e. $\overline{X}' < \sigma_1 < \overline{X}$, the ply failure is assumed to be resin induced. Consequently, the laminate loses its capability to support transverse and shear stresses, but remains to carry longitudinal stress. In this case, the constitutive matrix of the lamina becomes

$$[Q_1'] = \begin{bmatrix} E_{11} & 0 & 0 \\ 0 & 0 & 0 \\ 0 & 0 & 0 \end{bmatrix} \tag{12}$$

(2) If a ply fails with σ_1 exceeding the uniaxial strength of the lamina, the ply failure is caused by the fiber breakage and a total ply rupture is assumed. In this case, the constitutive matrix of the lamina becomes

$$[Q_1'] = \begin{bmatrix} 0 & 0 & 0 \\ 0 & 0 & 0 \\ 0 & 0 & 0 \end{bmatrix} \tag{13}$$

The material used in the numerical analysis is E-Glass/Epoxy composites. Its material properties and strengths are (Soden, Hinton and Kaddour, 1998):

(1) Material properties: E_{11}=45.6 GPa, E_{22}=16.2GPa, G_{12}=5.83 GPa, υ_{12}=0.278

$$S_{6666} = \begin{cases} 0\,GPa^{-3}, if\ 0 \le \gamma_{12} \le 0.006 \\ 9723.85(\gamma_{12} - 0.006)GPa^{-3}, if\ 0.006 \le \gamma_{12} < 0.007 \\ -3.56942 + 1899.03882\gamma_{12}\ GPa^{-3}, if\ 0.007 \le \gamma_{12} < 0.04 \end{cases}$$

(2) Ultimate strengths: X_{ut}=1280 MPa, X_{uc}=-800 MPa, Y_{ut}=40 MPa, Y_{uc}=-145 MPa, S=72 MPa

The variable shear parameter, S_{6666}, is obtained by curve fitting from the pure shear test data (Soden, Hinton and Kaddour, 1998), as shown in Fig. 7.

During a finite element analysis, the constitutive matrix of composite materials at the integration points of shell elements must be calculated before the stiffness matrices are assembled from the element level to the structural level. For composite materials, the incremental constitutive equations of a lamina in the element coordinates (x,y,z) can be written as:

$$\Delta\{\sigma\} = [Q_1]\Delta\{\varepsilon\} \tag{14}$$

$$\Delta\{\tau_t\} = \{Q_2\}\Delta\{\gamma_t\} \tag{15}$$

where $\Delta\{\sigma\} = \Delta\{\sigma_x,\sigma_y,\tau_{xy}\}^T$, $\Delta\{\tau_t\} = \Delta\{\tau_{xz},\tau_{yz}\}^T$, $\Delta\{\varepsilon\} = \Delta\{\varepsilon_x,\varepsilon_y,\gamma_{xy}\}^T$, $\Delta\{\gamma_t\} = \Delta\{\gamma_{xz},\gamma_{yz}\}^T$, and

$$[Q_1] = [T_1]^T [Q_1'][T_1] \tag{16}$$

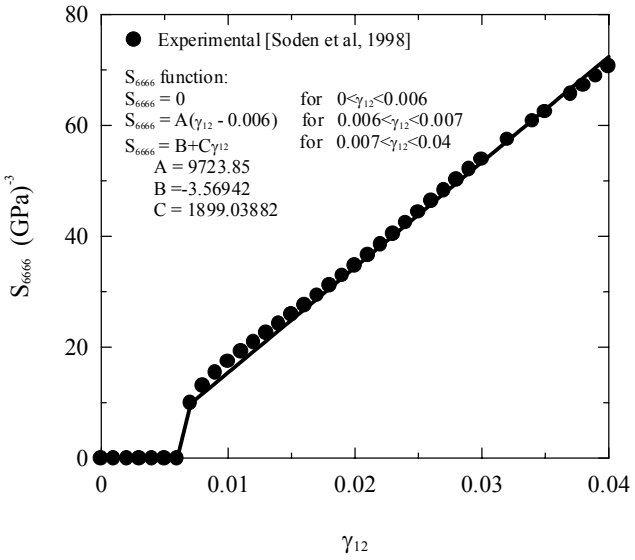

Fig. 7 Nonlinear shear parameter S_{6666} vs. various shear strains γ_{12} for E-glass/MY750/HY917/DY063 epoxy lamina

$$[Q_2] = [T_2]^T [Q_2'][T_2] \tag{17}$$

$$[T_1] = \begin{bmatrix} \cos^2\theta & \sin^2\theta & \sin\theta\cos\theta \\ \sin^2\theta & \cos^2\theta & -\sin\theta\cos\theta \\ -2\sin\theta\cos\theta & 2\sin\theta\cos\theta & \cos^2\theta - \sin^2\theta \end{bmatrix} \tag{18}$$

$$[T_2] = \begin{bmatrix} \cos\theta & \sin\theta \\ -\sin\theta & \cos\theta \end{bmatrix} \tag{19}$$

The θ is measured counterclockwise from the element local x-axis to the material 1-axis (Fig. 6). Assume $\Delta\{\varepsilon_o\} = \Delta\{\varepsilon_{xo},\varepsilon_{yo},\gamma_{xyo}\}^T$ are the incremental in-plane strains at the mid-surface of the shell section and $\Delta\{\kappa\} = \Delta\{\kappa_x,\kappa_y,\kappa_{xy}\}^T$ are its incremental curvatures. The incremental inplane strains at a distance z from the mid-surface of the shell section become

$$\Delta\{\varepsilon\} = \Delta\{\varepsilon_0\} + z\Delta\{\kappa\} \tag{20}$$

Let h be the total thickness of the composite shell section, the incremental stress resultants, $\Delta\{N\} = \Delta\{N_x,N_y,N_{xy}\}^T$, $\Delta\{M\} = \Delta\{M_x,M_y,M_{xy}\}^T$ and $\Delta\{V\} = \Delta\{V_x,V_y\}$, can be defined as:

$$\begin{Bmatrix} \Delta\{N\} \\ \Delta\{M\} \\ \Delta\{V\} \end{Bmatrix} = \int_{-h/2}^{h/2} \begin{Bmatrix} \Delta\{\sigma\} \\ z\Delta\{\sigma\} \\ \Delta\{\tau_t\} \end{Bmatrix} dz \tag{21}$$

Substituting Eqs. (14), (15) and (20) into the above expression, one can obtain the stiffness matrix for the fiber composite laminate shell at the integration point as shown in Eqs. (22), where [0] is a 3 by 2 null matrix.

$$\begin{Bmatrix} \Delta\{N\} \\ \Delta\{M\} \\ \Delta\{V\} \end{Bmatrix} = \int_{-h/2}^{h/2} \begin{bmatrix} [Q_1] & z[Q_1] & [0] \\ z[Q_1] & z^2[Q_1] & [0] \\ [0]^T & [0]^T & [Q_2] \end{bmatrix} \begin{Bmatrix} \Delta\{\varepsilon_0\} \\ \Delta\{\kappa\} \\ \Delta\{\gamma_t\} \end{Bmatrix} dz \tag{22}$$

VERIFICATION OF THE PROPOSED MATERIAL CONSTITUTIVE MODELS

The validity of the material models for steel, concrete (Hibbitt, Karlsson, and Sorensen, 2002) and FRP (Lin and Hu, 2002) has been verified individually by testing against experimental data and is not duplicated here. The validity of the these material models to simulate the composite behavior of reinforced concrete slab strengthened by FRP is examined in this section by comparing with the result of slab experiment performed by Mosallam and Mosalam (2003). The dimensions of the test slab are given in Fig. 8.

The slab is subjected to a uniform static pressure applied to the bottom surface of the slab up to failure. The top surface will subject to tensile stress. Tension (top) reinforcement consisted of #3 (9.52 mm) at 305 mm (12-inch) equal spacing in the two orthogonal directions of the test slab with 13 mm (0.5-inch) cover. Grade 60 reinforcing steel was used. The yielding stress is 413.7 MPa (60 ksi). The stress-strain relation of the reinforcing bar is assumed to be a bilinear model to consider the strain hardening behavior. Its elastic modulus in initial linear elastic region is assumed to be 199.9 GPa (29000 ksi) and the elastic modulus in strain hardening region is smaller than that of the initial elastic region by a factor of 33 (Mosallam and Mosalam, 2003). The compressive strength and the Poisson's ratio of concrete are $f_c' = 34.47$ MPa (5 ksi) and ν_C=0.2.

Two FRP layers spaced at 457 mm (18 inches) are adhered to the top side with their fiber directions oriented in the two orthogonal directions of the slab. At the intersection regions of the staggered unidirection laminates from the two directions, bidirectional fiber architecture, i.e. a 90°/0°/90°/0° lamination schedule was formed. Each FRP layer is 0.58 mm (0.023 inch) in thickness and with tensile strength X_{ut}=1208.7 MPa and modulus E_{11}=100.75 GPa (Mosallam and Mosalam, 2003). To take the Tsai-Wu criterion into account, the following parameters are also assumed: E_{22}=1 GPa, G_{12}=1 GPa, X_{uc}=-12 MPa, Y_{ut}=12 MPa, Y_{ut}=-12 MPa, S=12 MPa, S_{6666}=0, υ_{12}=0.3. It is necessary to point out that a parameter $\varepsilon_{utf,}$ ultimate strain of FRP in fiber direction, is used. The value of ε_{utf} is assumed to be 0.5% (Yang, 2003). In addition, due to limited experimental data, the above material properties and strengths are assumed about 1% of the corresponding values in the fiber direction.

The slab has two planes of symmetry. These two planes are formed by cutting the slab through its two center lines of the top surface. Due to symmetry, only 1/4 portion of the slab is analyzed and symmetric boundary conditions are placed along the two symmetric planes. In the finite element analysis, 8-node shell elements (six degrees of freedom per node) are used to model the reinforced concrete slabs and the fiber-reinforced plastics. The 1/4 RC slab mesh has 25 shell elements and the fiber-reinforced plastics has 21 shell elements in total. The FRP shell elements are attached to the top surface of the concrete slab directly and perfect bonding between FRP and the concrete is assumed.

Figure 9 shows the total applied load versus deflection curves of the slab at the mid-point. It can be observed that the correlation is quite good between the numerical result and the experimental data. One curve represents the RC slab and the other represents the retrofitted slab. The predicted ultimate total applied load 215.2 kN of the RC slab is in good agreement with the experimental ultimate load 219.3 kN. The error is

only about 2%. The others of retrofitted slab is 451.7 kN which has about 4% error with respect to the experimental ultimate load, 434.3 kN. Hence, the proposed material constitutive models are proved to be able to simulate the composite behavior of reinforced concrete beam strengthened by FRP correctly.

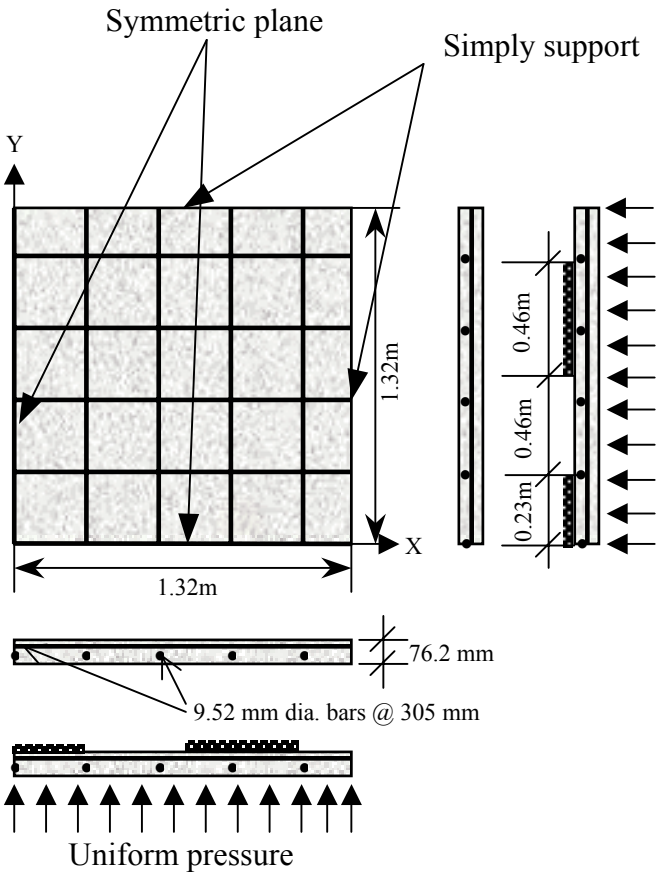

Fig. 8 Details of test slab (1/4 model)

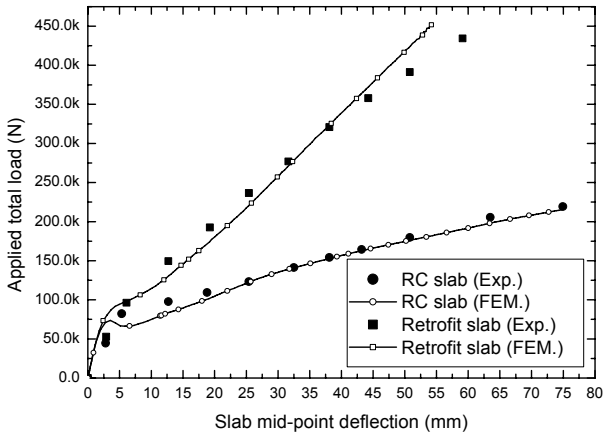

Fig. 9 Comparisons between numerical and experimental data

NUMERICAL ANALYSIS

In the numerical analyses, simply supported square reinforced concrete slabs are considered. These slabs again have two planes of symmetry and the geometries of them are the same as those in the verification test. The dimensions of the RC slabs are shown in Fig. 8.

Three types of strengthening schemes are analyzed. First, cross retrofit along two symmetric axes of the slab is considered and the strengthened area is 6048 cm^2, as shown in Fig. 10 Type Ⅰ. Second, retrofit along the diagonal of RC plate is used and the retrofitted area is 6048 cm^2, as shown in Fig. 10 Type Ⅱ. The last, retrofit perpendicular to the diagonal of RC slab and the strengthened area is also 6048 cm^2, as shown in Fig. 10 Type Ⅲ. The total strengthened area of above three cases is the same. The thickness of each FRP layer is 0.1 mm. A total of two layers of FRP strips are bonded to the tension side of the slab and the fibers are all parallel to the longitudinal direction of the strip. As a result, there are 4 layers of FRP with [90/0/90/0] layup on the overlap of the first retrofit scheme and with [45/-45/45/-45] layup on the overlap of the other two types. The fiber angle of the lamina is measured counterclockwise from the X-axis to the Y-axis.

Since X and Y axes are symmetric lines of the slab, only one fourth of slab is analyzed and symmetric boundary conditions are placed along the two symmetric planes. In the finite element analysis, 8-node shell elements (six degrees of freedom per node) are used to model reinforced concrete slabs. There are 25 elements used in slabs model. The modeling of FRP is different from each other because the strengthened types may form a 45 degree or -45 degree with the X axis. So, both triangular and quadrilateral shell elements (six degrees of freedom per node) are used to model the FRP. The FRP shell elements are attached to the tensile surface of the concrete slab directly and perfect bonding between FRP and the concrete is assumed.

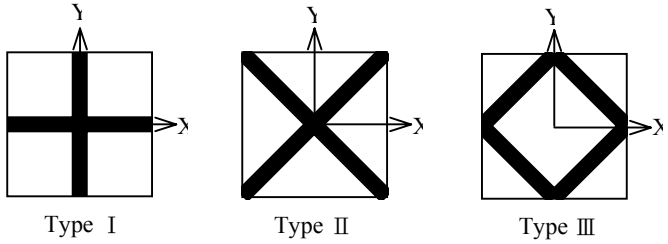

Fig. 10 Three retrofit types in discussion

The applied total load versus the central deflection of the slab of the three cases are shown in Fig. 11. The ultimate loads of the reinforced concrete slab and three retrofit cases are listed in the Table 1.

Table 1. Ultimate loads P_u and the increase in P_u (%)

	RC slab	Type Ⅰ	Type Ⅱ	Type Ⅲ
P_u (kN)	238.9	321.5	241.2	252.3
Increase in P_u (%)	–	34.6	0.96	5.6

From the numerical results, the stiffness and strength of the slabs increase when FRP laminates are adhered to the tensile plane of the slabs. The increasing in P_u of Type Ⅱ is only 0.96%. This indicates that the ultimate load of the reinforced concrete slab is almost the same after strengthening. Only stiffness increases in this type. This is because the fiber directions are parallel to the yield lines of the slab. The transverse strength of laminate is quite lower than that in the longitudinal direction. Once the concrete cracks, the FRP can not take over the tensile force

from the slab and fails quickly.

Type Ⅰ is the best strengthening type among them. Its ultimate load P_u is higher than that of the reinforced concrete slab by 34.6%. Two cross retrofitted lines are along the direction of the maximum bending stress and the advantages of FRP strips can be raised.

The stiffness of Type Ⅲ is almost the same with that of Type Ⅱ. The increasing in P_u is 5.6%, a little higher than that of Type Ⅱ. The drawback of this strengthening scheme is dismissing the place where the maximum bending moments take place.

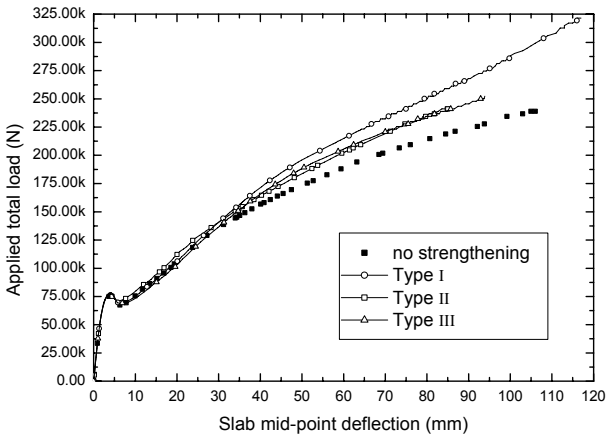

Fig. 11 Load-deflection curves of reinforced concrete plate with retrofit schemes.

CONCLUSION

By considering the proper constitutive models, we present a rational numerical model to analyze the reinforced concrete structures strengthened by FRP. In verification, the behaviors of both RC slab and retrofitted slab are predicted accurately against the experimental data. Owing to the small failure shear strain of the composite plates, the material nonlinearity of FRP in in-plane shear stress-strain relation dose not influence the behavior of the composite square slabs at all. If longitudinal directions of the FRP coincide with the yielding lines of RC slabs, the ultimate load of the slab may not increase too much. The best strengthening scheme can be achieved if the longitudinal directions of the FRP and the directions of the maximum bending stress are in parallel.

REFERENCES

ACI Committee 318 (1999). Building Code Requirements for Structural Concrete and Commentary (ACI 318-99), American Concrete Institute, Detroit, Michigan.

ASCE Task Committee on Concrete and Masonry Structure. State of the art report on finite element analysis of reinforced concrete, ASCE, 1982.

Chen, WF (1982). Plasticity in reinforced concrete, McGraw-Hill.

Hahn, HT, and Tsai, SW (1973). "Nonlinear elastic behavior of unidirectional composite laminae," *J Compos Matls*, Vol 7, pp 102-118.

Hibbitt, Karlsson, and Sorensen, Inc (2002). ABAQUS Theory Manual, User Manual and Example Manual, Version 6.3, Providence, Rhode Island.

Hu, HT, Lin, FM, and Jan, YY. "Nonlinear Finite Element Analysis of Reinforced Concrete Beams Strengthened by Fiber-Reinforced Plastics," *Comps Struct*, Vol. 63, No. 3-4, February-March 2004, pp. 271-281.

Hu, HT, and Schnobrich, WC (1989). "Constitutive modelling of concrete by using nonassociated plasticity," *J Matls in Cil Engrg*, ASCE, Vol1, No 4, pp 199-216.

Hu, HT, and Schnobrich, WC (1990). "Nonlinear analysis of cracked reinforced concrete," *ACI Struct J*, Vol 87, No 2, pp 199-207.

Kupfer, H, Hilsdorf, HK, and Rusch, H (1969). "Behavior of concrete under biaxial stresses," *ACI J*, Vol 66, pp 656-666.

Jones, RM, and Morgan, HS (1977). "Analysis of nonlinear stress-strain behavior of fiber-reinforced composite materials," AIAA Journal, Vol 15, pp 1669-1676.

Lin, WP, and Hu, HT (2002)., "Nonlinear Analysis of Fiber-Reinforced Composite Laminates Subjected to Uniaxial Tensile Load," *J Compos Matls*, Vol 36, No 12, pp 1429-1450.

Lin, WP, and Hu, HT (2002)., "Parametric Study on the Failure of Fiber-Reinforced Composite Laminates under Biaxial Tensile Load," *J Compos Matls*, Vol 36, No 12, pp 1481-1504.

Mosallam, AS, and Mosalam, KM (2003). "Strengthening of two-way concrete slabs with FRP composite laminates," *Construction and Building Materials*, Vol 17, pp 43-54.

Rabinovitch, O, and Frostig, Y (2003). "Experiments and analytical comparison of RC beams strengthened with CFRP composites," Composites: Part B, Vol 34, pp 663-677.

Saadatmanesh, H, and Ehsani, MR (1991). "RC beams strengthened with FRP plates II: analysis and parametric study," *J Struct Engng*, ASCE, Vol 117, No 11, pp 3434-3455.

Saenz, LP (1964). "Discussion of "Equation for the stress-strain curve of concrete" by Desayi P and Krishnan S," *ACI J*, Vol 61, pp 1229-1235.

Tsai, SW, and Wu, EM (1971). "A general theory of strength for anisotropic materials," *J Compos Matls*, Vol 5, pp58-80.

Yang, CJ. "The Applications of Carbon Fiber Composite on Strengthening the RC Slabs Structure," MS thesis, Department of Construction Engineering, National Taiwan University of Science and Technology, Taipei, Taiwan, ROC, 2003, (in Chinese).